Indentation damage evaluation on metal-coated thin-films stacked structure

Alfred Yeo
Operation Backend Development, Infineon Technologies Asia Pacific Pte Ltd, Singapore 349253; and School of Mechanical and Aerospace Engineering, Nanyang Technological University, Singapore 639798

Mao Liu and Kun Zhou[a)]
School of Mechanical and Aerospace Engineering, Nanyang Technological University, Singapore 639798

(Received 27 May 2015; accepted 26 August 2015)

A micro-indentation system integrated with an acoustic emission (AE) sensor is used as a damage test method for crack detection of the specimen during the indentation loading–unloading cycle. The specimens investigated are the Si die, and various stacked structures of metallization (Al or Cu) deposited over the dielectric layers (SiO_2 or Si_3N_4) on the Si substrate. The 1st AE event detected during the loading stage corresponded to the 'pop-in' observation in the force–displacement curve, which was related to the brittle cracking in the dielectric or Si substrate. However, during unloading, a 2nd AE event was detected, but no "pop-out" was observed, which was mainly due to the delamination between the dielectric and Si substrate. It was also found that for Si die, "pop-out" was observed without any AE event during the unloading stage, which was related to the Si phase transformation. This observation is unique to sharp indenter tip but not for a blunt indenter tip.

I. INTRODUCTION

An instrumented indentation equipment, also known as the depth-sensing indentation, has been increasingly being used to probe the mechanical response of materials from metals and ceramics to polymeric engineering materials.[1–39] Due to the ease and speed of the indentation testing, this method has gained popularity in assessing the mechanical properties of thin films and small volume specimens, as motivated by their modern applications in microelectronics, microelectromechanical systems (MEMSs), biomaterials, etc.[3–7,15–18,22–25,29–35]

The most fundamental measures made by an instrumental indentation system are force and displacement, which describe the mechanical behavior of the material during the indentation process. The two measurements are typically coupled in the system through support springs. The additional levels of control, sensitivity, and data acquisition offered by depth-sensing indentation systems have resulted in numerous advances in materials science, particularly on fundamental mechanisms of mechanical behavior at the micrometer and even submicrometer length scales. As such, it can be used to determine not only the hardness but also the elastic modulus E, yield strength Y, strain-hardening exponent, fracture toughness, energy absorption, and other time-dependent properties.[1–39] All these material properties depend on the interpretation and analysis of the force–displacement F–d results, coupled with the analytical and modeling methodologies. The material evaluated is usually either a bulk or a hard-coating thin film on a substrate, and there is limited publication discussing on the soft coating thin-film, i.e., metallization, on the stacked structure, where cracking normally occurs at the brittle layer underneath the ductile metallization. Since the cracking of the brittle layer is not visible and difficult to detect, it is important to understand and predict the damage behavior and its occurrence, especially in the application of interconnection assembly process for microelectronics devices and MEMSs.[40,41]

This paper presents an indentation damage test system that uses an instrumented micro-indentator together with an acoustic emission (AE) sensor for crack detection in the bare Si and various thin-films stacked specimens, i.e., metal coating over dielectric layer on the Si substrate, during indentation loading–unloading cycles. The specimens are then examined in detail by both delayering and cross-sectioning failure analysis techniques. Different AE signal features are extracted and compared with regard to the quality of signal transmission. The indentation F–d responses are measured, where the onset crack forces F_{cr} and displacements d_{cr} are determined corresponding to the occurrence of the AE events, and subsequently discussed with the observed failure mode and damage location.

II. EXPERIMENTAL

The experimental set-up of the damage test system consists of an instrumented micro-indentation equipment

Contributing Editor: Sam Zhang
[a)]Address all correspondence to this author.
e-mail: kzhou@ntu.edu.sg
DOI: 10.1557/jmr.2015.278

 © Materials Research Society 2015

https://doi.org/10.1557/jmr.2015.278 Published online by Cambridge University Press

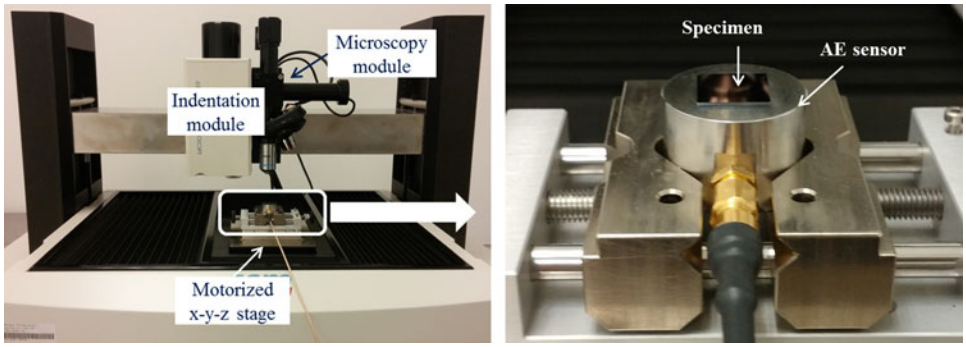


FIG. 1. A damage test system set-up.

and a piezo-electric AE sensor, as depicted in Fig. 1. To examine the mechanical load threshold of the thin-films stacked specimen, only the backside of the Si substrate was in contact with the AE sensor, where the indentation load was applied directly and normally on the top surface of the specimen, with a 50 μm-diameter round-ended diamond tip. During testing, the *F–d* response and the AE signal were recorded simultaneously. When a crack event occurred in the specimen, the emitted ultrasonic wave reflected as a short burst or spike in the sensing output voltage.

A. Instrumentation

AE testing is a passive and receptive technique that analyzes the ultrasound pulses emitted by a defect right in the moment of its occurrence resulted from an external stimulus. Therefore, AE analysis is an appropriate technique for determining the mechanical load limit of the test specimen, by "listening" to the defects upon their occurrence in real-time. Most AE sensors rely on the piezo-electric effect to transform a surface motion or displacement into an electrical signal, and these sensors are usually very sensitive and do not saturate. In this work, a resonant type of AE sensor with a working frequency range of 100–450 kHz was connected to the Vallen AMSY-6 system for signal processing and analysis. The AE sensor was positioned firmly in a fixture on the universal adapter, which was mounted on the *x–y–z* motorized stage of the micro-indentation equipment, to detect any damage occurrence in the specimen during the indentation loading–unloading cycle.

In this experiment, a fine setting mode was selected that provided a normal load range of 0.05–10 N at a maximum depth of 100 μm, using the same loading and unloading rate at three different conditions, i.e., 0.1, 0.5, and 1 N/min. The system was equipped with a special feature known as a reference ring that was attached to the indenter holder, which served two purposes in reducing the thermal drift on the depth signal and eliminating the system compliance. During the indentation loading and unloading cycle, both the *F–d* response and AE signal

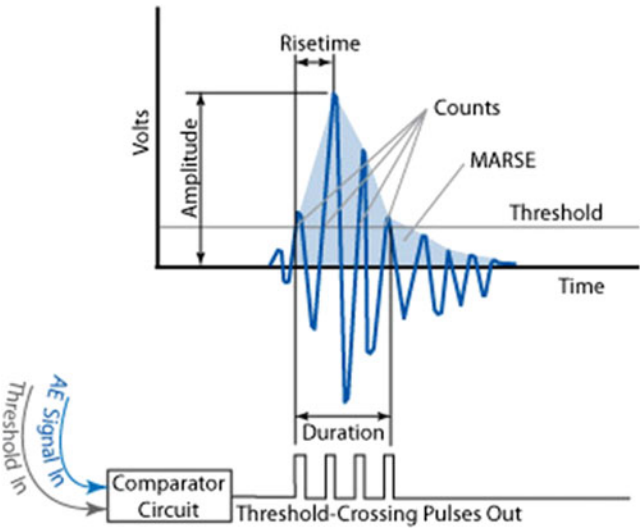


FIG. 2. AE features of transient signals.

TABLE I. Geometry specifications of the specimens.

Specimen	Metallization layer thickness (μm)	Target dielectric thickness (μm)	Substrate thickness (μm)
Si	...	...	500 ± 20
Al–SiO_2–Si	1 ± 0.2	1 ± 0.2	500 ± 20
Al–Si_3N_4–Si	1 ± 0.2	1 ± 0.2	500 ± 20
Cu(Ti)–SiO_2–Si	1 ± 0.2	1 ± 0.2	500 ± 20
Cu(Ti)–Si_3N_4–Si	1 ± 0.2	1 ± 0.2	500 ± 20

were monitored real-time in the Vallen acquisition program until the 1st AE event occurred, and the indenter was then retracted to its original position. Both the *F–d* response and AE signal were integrated and synchronized, where damage parameters such as the onset crack force F_{cr} and displacement d_{cr} were calculated, which corresponded to the AE event detected. In addition, AE features such as amplitude, arrival or rise time, duration time and energy could also be determined (see Fig. 2). To determine the AE threshold setting, the AE signal was monitored for 10 min, while the

https://doi.org/10.1557/jmr.2015.278 Published online by Cambridge University Press

micro-indentation machine is turned on without performing any damage testing. The maximum AE magnitude recorded was then defined as the threshold voltage used in the AE event detection. The input AE threshold used in this damage test was 57.6 dB, the data sampling frequency was 10 MHz, and the digital filter setting was 95–850 kHz.

B. Specimen preparation

The preparation of the thin-films stacked specimen was carried out using the standard wafer fabrication process on a 100 mm-diameter wafer. The Si wafer was first going through a plasma-enhanced chemical vapor deposition process, where a homogenous layer of dielectric layer (SiO_2 or Si_3N_4) was deposited on one

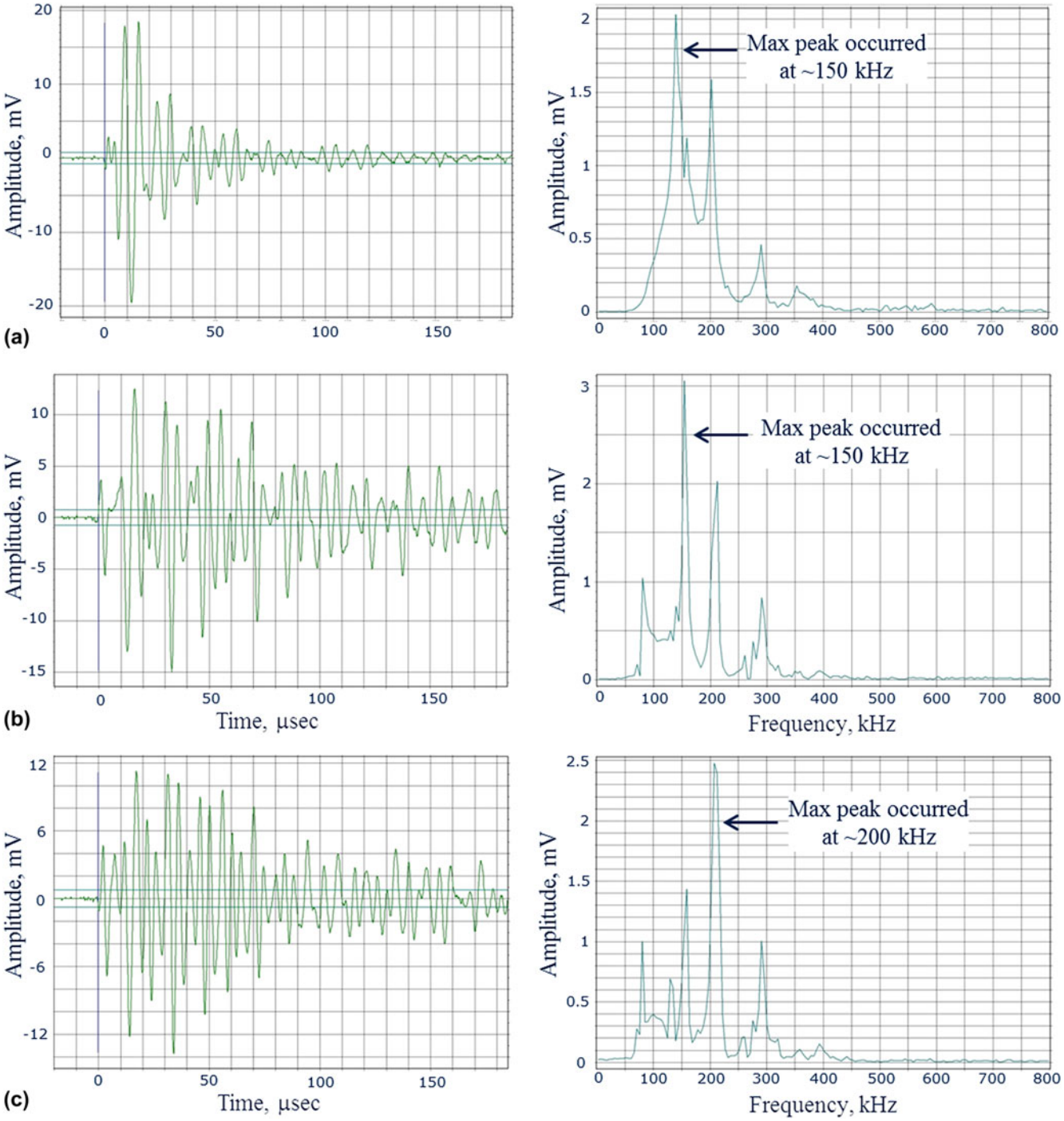


FIG. 3. Time and frequency responses of the first AE event occurrence for Si die: (a) with couplant medium, the maximum peak at ~150 kHz, (b) without couplant medium, the maximum peak at ~150 kHz, and (c) without couplant medium, the maximum peak at ~200 kHz.

https://doi.org/10.1557/jmr.2015.278 Published online by Cambridge University Press

side of the Si wafer surface. The Al or Cu metallization layer was then sputtered over the dielectric layer. However, a Ti layer of ~50 nm was required prior to the Cu deposition for adhesion purpose. Lastly, the wafer was sawn mechanically into a 10 mm × 10 mm die size. Table I presents the geometrical information of the specimens used in this work.

III. RESULTS AND DISCUSSION

The indentation damage test was performed at the room temperature (25 °C) on five different specimens listed in Table I. A minimum of 20 indentation tests was conducted on the five different specimens, followed by a post-mortem analysis, examining both the planar and cross-section areas of the indentation region. The indented surface of the top metallization layer was usually removed by wet chemical etchant (i.e., mixture of acids) to expose the dielectric SiO_2 or Si_3N_4 layer, and followed by rinsing the specimens with de-ionized water.[41] This delayering failure analysis technique only revealed the bulk material cracking or damage on the surface of the dielectric layer. To examine for any interfacial crack or delamination within the stacked structure, the cross-sectioning approach using focused ion beam (FIB) and scanning electron microscopy (SEM) technique was used.

A. AE signal quality test

Ideally, a couplant medium (between the specimen and the AE sensor) should be easily applicable and removable from the sensor without affecting the loading process, while possessing excellent acoustic impedance, thus providing a good signal-to-noise ratio. Nail polish that consisted of a film-forming polymer dissolved in a volatile organic solvent was then used as a couplant medium.

It was found that the measurement of the Si die with and without the couplant medium was independent of the loading and unloading rate. Thus, Fig. 3 shows only the time and frequency responses of the first AE event occurrence at the 1 N/min load rate. Figure 3(a) shows that a clear distinct peak amplitude consistently occurred at ~150 kHz for the Si die with couplant medium, but two different maximum amplitudes (~150 and ~200 kHz) occurred in the case without it [Figs. 3(b) and 3(c)]. The failure mode in the Si die was similar for both with and without the couplant medium, as shown in Fig. 4, where the ring crack and sometimes the radial crack were observed on the indented Si surface, and the subsurface cracking was also found in the Si from the FIB/SEM analysis.

Different AE parameters are extracted and compared in Fig. 5. Generally, the introduction of nail polish as a couplant medium yielded a lower, consistent AE rise and duration. In additional, smaller standard deviations of the AE peak voltage and energy were also observed. It was found that a comparable mechanical response was measured for both Si dies with and without the couplant medium, which implies that the use of nail polish will not affect the mechanical result of the indentation.

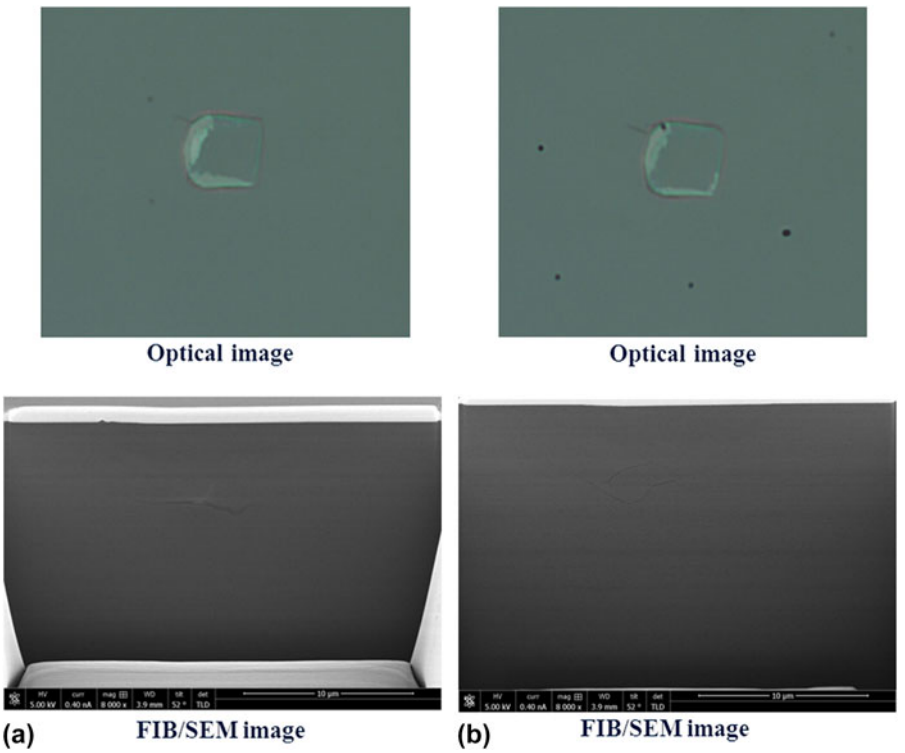


FIG. 4. Failure modes of the Si die: (a) with and (b) without couplant medium.

https://doi.org/10.1557/jmr.2015.278 Published online by Cambridge University Press

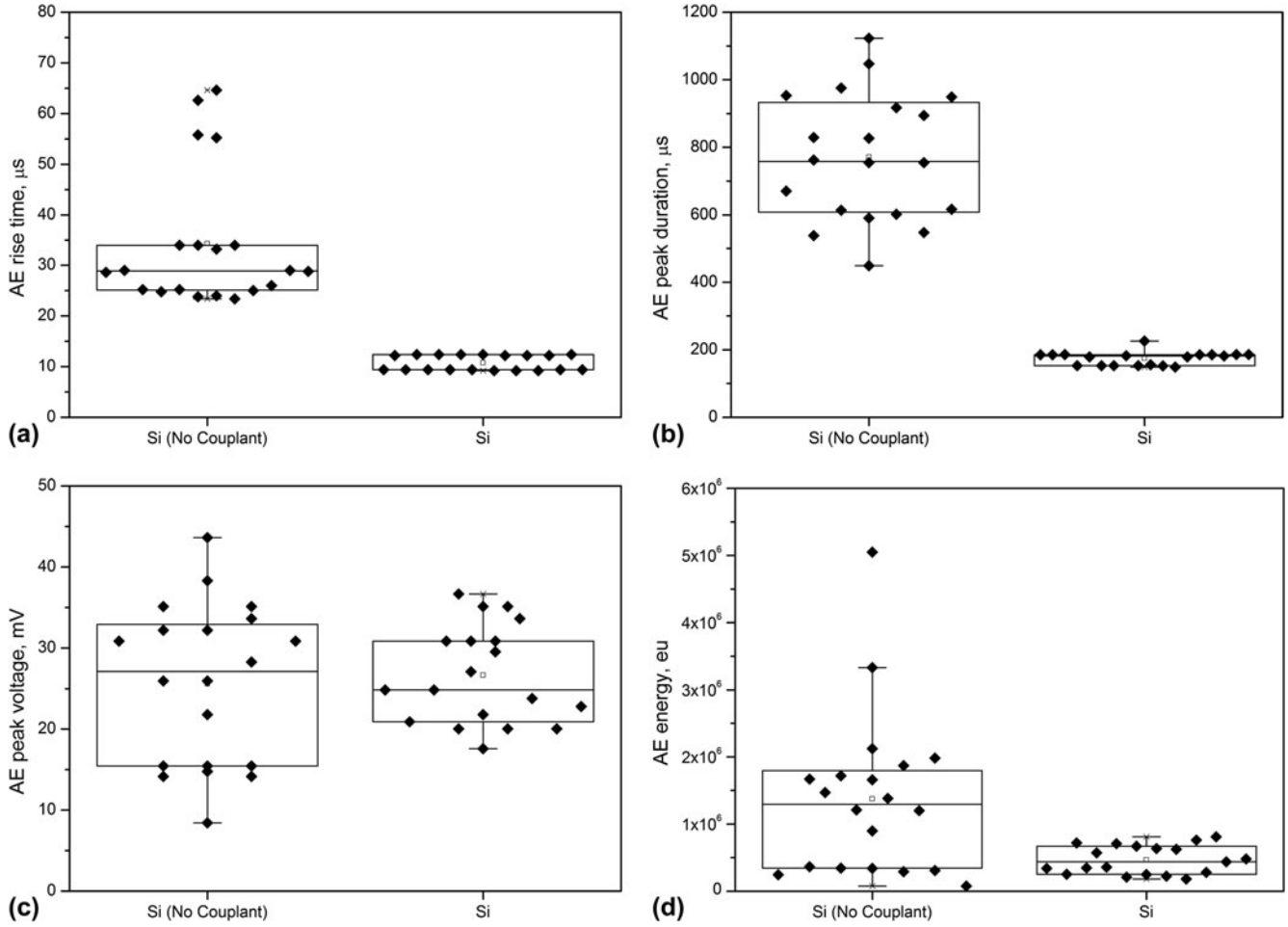


FIG. 5. AE signal results of the Si die with and without couplant medium: (a) rise time, (b) duration time, (c) peak voltage, and (d) energy.

Nail polish was applied in the subsequent damage test. Besides a good quality of AE signal detection, the specimen was able to adhere firmly on the AE sensor especially during the *x*–*y*–*z* motorized stage movement.

B. Damage test on the metal-coated stacked structure

The mechanical responses of the thin-films metal stacked specimens are presented in Fig. 6, together with the results of the Si die for comparison. The first AE event corresponded to the "pop-in" observation in the *F*–*d* curve shown in Fig. 6(a). This "pop-in" was a result of sudden increase in the distant traveled by the indenter when the cracking of the specimen occurred (for a load-controlled indentation) before reaching another resistance point. This suggests that the stored energy in the specimen converted from the work of indentation was released by fracture, and the specimen lost its structural integrity and stiffness at the instance of "pop-in" occurrence. A new stiffness would usually be measured after the "pop-in" if the indenter continued the loading process on the damaged specimen. However, in this test the indenter was retracted at the same rate as the loading process after the "pop-in" event.

The mean onset crack forces measured were 1.2, 1.9, 2.0, 1.3, and 1.5 N for the Si, Al–SiO_2–Si, Cu–SiO_2–Si, Al–Si_3N_4–Si, and Cu–Si_3N_4–Si specimens respectively for different loading rates [Fig. 6(b)]. The results show that the measured onset crack forces were independent of the loading rate used in this indentation damage test. It was also observed that the onset crack forces strongly depended on the dielectric material used, as compared to the metallization layer. To validate the accuracy of the crack detection means by the AE sensor, all thin-films stacked specimens were tested at 1.1 N, a force closed to the minimum F_{cr} of the Si die. There was no AE event detected and no damage was observed. In addition, this shows that the thin-films stacked layers enhanced the indentation damage threshold of the Si die. Generally, the specimens with SiO_2 dielectric yielded a higher 1st AE peak voltage and energy [(Figs. 7(a) and 7(b)], which also corresponded to a higher onset crack force measured.

https://doi.org/10.1557/jmr.2015.278 Published online by Cambridge University Press

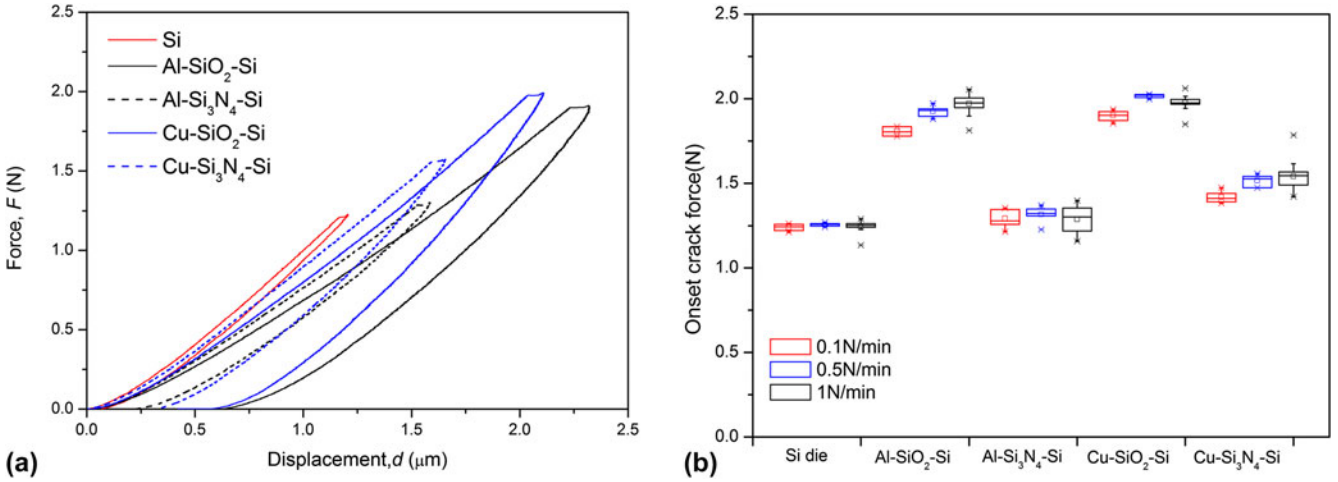


FIG. 6. Mechanical responses of the metal-coated thin-films stacked specimens: (a) indentation *F–d* response, and (b) onset crack forces at different loading rates.

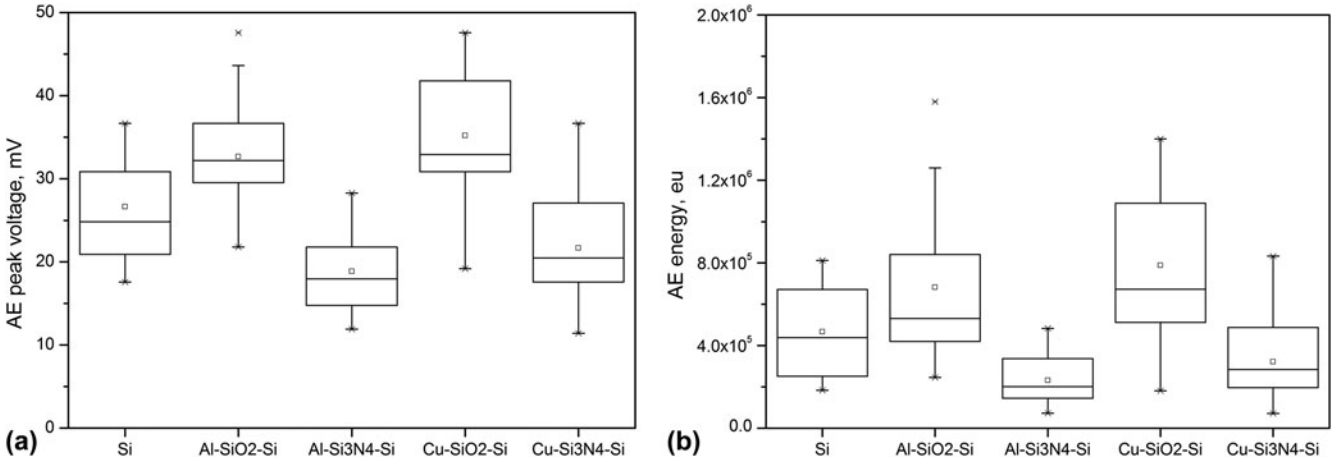


FIG. 7. AE signal results of the Si die and various thin-films stacked specimens: (a) peak voltage, and (b) energy.

The AE time and frequency spectrum responses of the thin-films stacked specimens were quite similar, as compared to the Si die, where the maximum peak voltage of the 1st AE event usually occurred at ~150 kHz [Figs. 3, 8 and 9]. However, it was found that a second AE event sometimes occurred during the unloading stage at 0.1–0.2 N, as shown in Figs. 8 and 9 for the cases of Al–SiO_2–Si and Cu–SiO_2–Si specimens, respectively. Both the first and second AE peak signals consistently occurred at 150 kHz, where the first peak voltage was always higher than the second one. Interestingly, there was no AE event detected during the unloading cycle for the case of bulk Si and metal-coated Si_3N_4 dielectric specimens.

No cracking was observed in the top metallization layers for all the specimens after the indentation damage test, except for a round indented mark and a pile-up around the indented area. However, delayering of top metallization revealed peeling and radial cracking on the SiO_2 surfaces, as shown in Figs. 10(a) and 10(c). Ring and radial cracking were observed on the Si_3N_4 surfaces for the Al metallization specimens [Fig. 10(b)], and only radial cracking was observed for the Cu metallization specimens [Fig. 10(d)]. This suggests that the softer Al experienced a larger pile-up during indentation, which could potentially induce a ring crack on the Si_3N_4 layer underneath, as compared to the Cu metallization with a Ti adhesive layer.

The cross-sectioning of the specimen was examined by FIB/SEM analysis, as presented in Fig. 11. The metal-coated SiO_2 dielectric specimen demonstrated both the cone and subsurface cracking in the Si substrate [Figs. 11 (a) and 11(c)], and delamination between the SiO_2 and Si interface [Fig. 11(a)]. Furthermore, Figs. 10(a) and 10(c) show a partial "white-ring" at the perimeter of the imprinted SiO_2 surface, which could be a tell-tale sign of dielectric peeling or delamination. However, for the metal-coated Si_3N_4 dielectric specimen, only subsurface

https://doi.org/10.1557/jmr.2015.278 Published online by Cambridge University Press

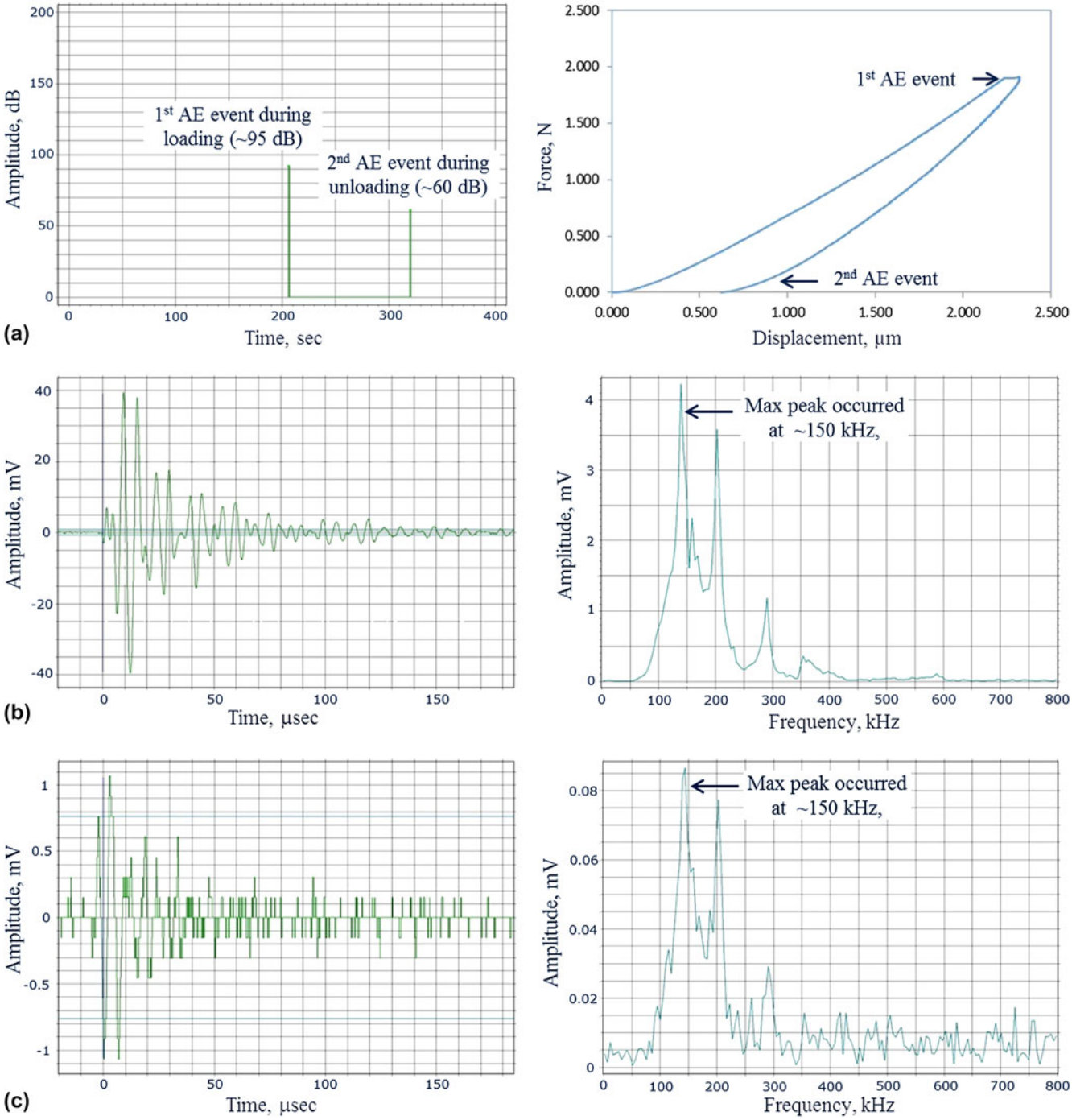


FIG. 8. Experiment results for Al–SiO_2–Si specimen: (a) time history graph and *F*–*d* curve, time and frequency spectrum plots of (b) the first AE and (c) the second AE events.

cracking was found in the Si substrate, and through-thickness cracking was observed in the Si_3N_4 layer [Figs. 11(b) and 11(d)]. It was also observed that the damage on Si_3N_4 surface was severe especially for Al metallization specimen, where the ring and radial cracks were obvious with longer crack lines as compared to SiO_2 [Fig. 10]. Hence, the delamination failure observed in the metal-coated SiO_2 dielectric specimen could be related to the second AE event detected during unloading of the indenter.

The SiO_2 has an elastic modulus ~5 times lower than Si_3N_4,[42] and hence from the SEM cross-sectioned images [Fig. 11], the SiO_2 dielectric layer experienced a larger deformation or "bending" without any through thickness

https://doi.org/10.1557/jmr.2015.278 Published online by Cambridge University Press

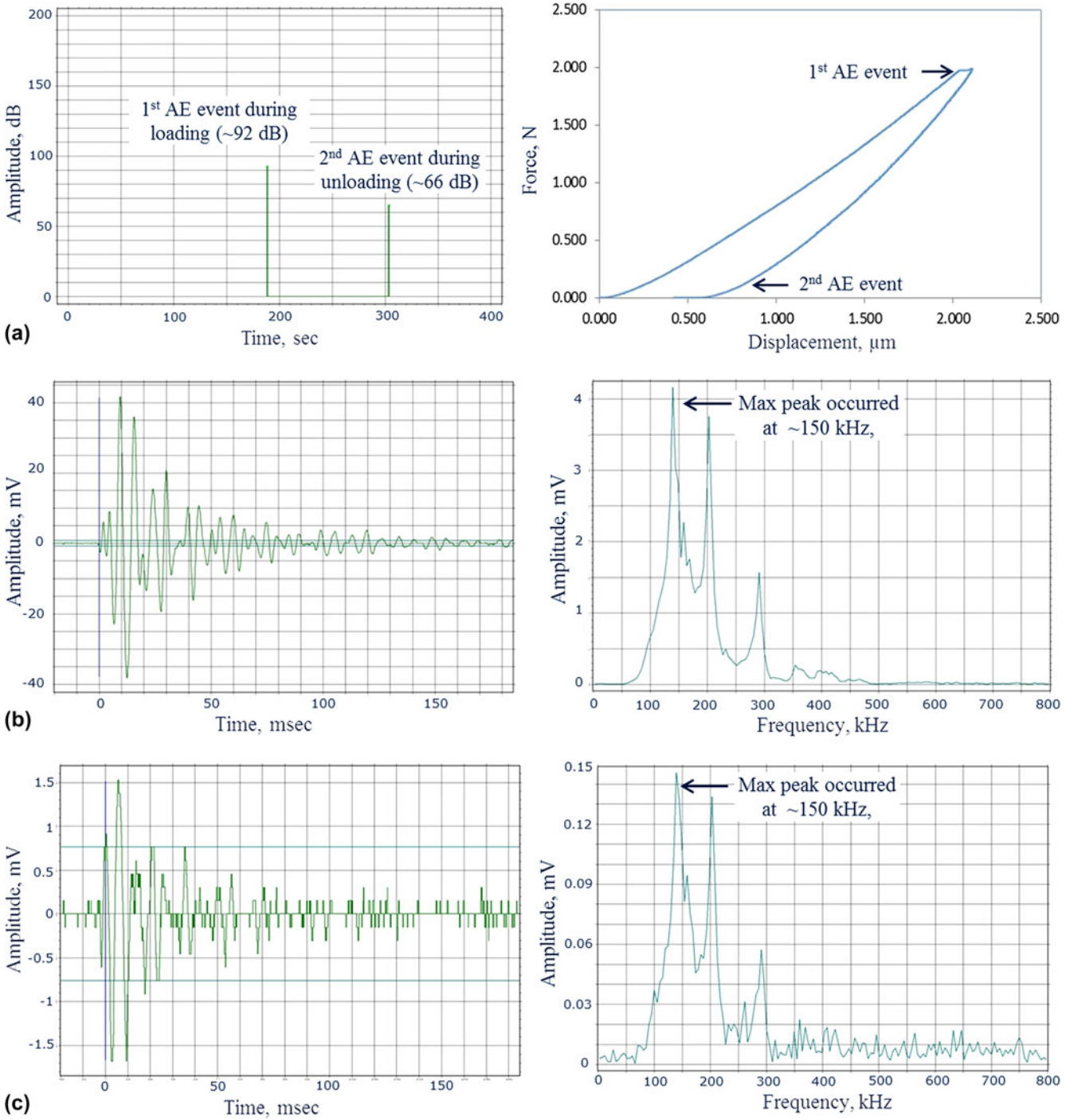


FIG. 9. Experiment results for Cu–SiO_2–Si specimen: (a) time history graph and *F–d* curve, time and frequency spectrum plots of (b) the first AE and (c) the second AE events.

cracking, as compared to the Si_3N_4 electric layer. This attested the lower onset crack force measured in the specimen with Si_3N_4 dielectric layer.

During the unloading stage, a larger elastic recovery of the metal-coated SiO_2 dielectric specimen was expected, which could result in a large strain energy released through delamination or interfacial cracking between the dielectric layer and the Si substrate. Furthermore, the detected peak voltage of the first AE event was much larger than that of the second one, which could shed lights on the occurrence of different damage modes during the loading and unloading stages. A large ultrasonic wave intensity or AE energy was usually emitted for a sudden cracking as observed in the brittle

https://doi.org/10.1557/jmr.2015.278 Published online by Cambridge University Press

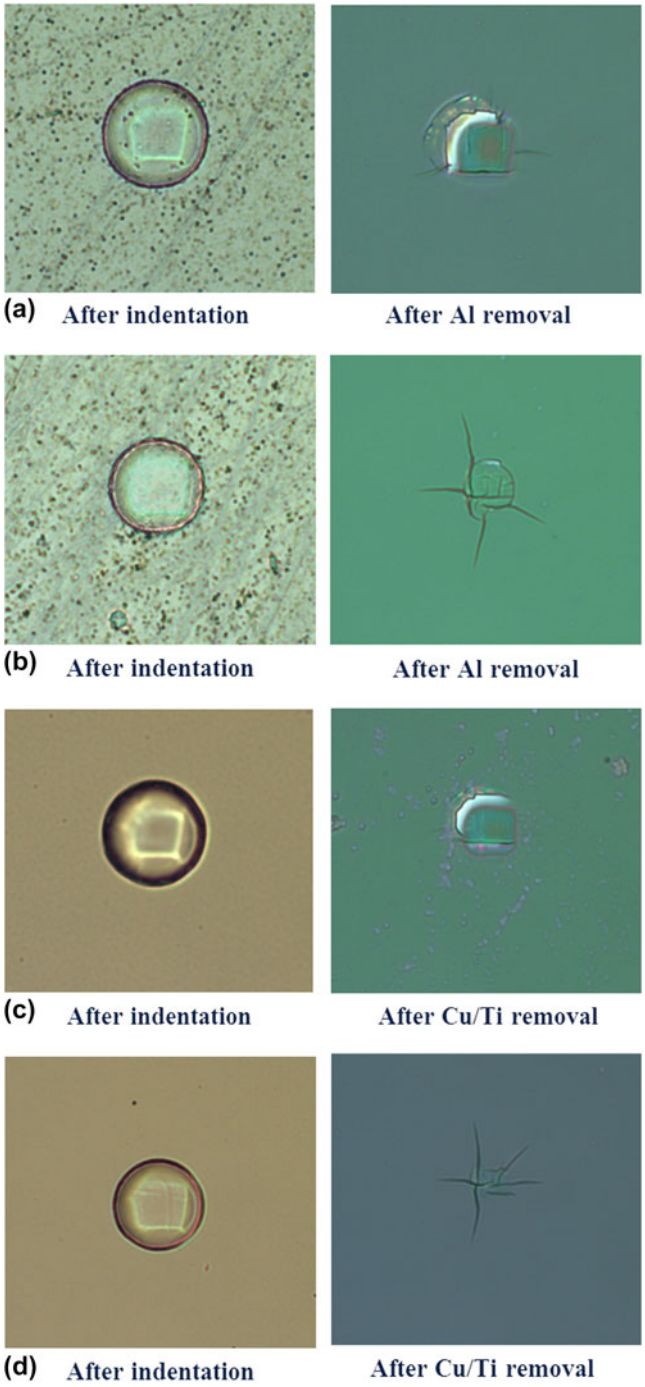


FIG. 10. Surface optical images of the damaged specimens after indentation tests: (a) Al–SiO_2–Si, (b) Al–Si_3N_4–Si, (c) Cu–SiO_2–Si, and (d) Cu–Si_3N_4–Si.

dielectric layer or the Si substrate during loading stage, and a weak AE energy might account for the delamination failure during the unloading stage. In addition, this weak AE energy detected in the second AE event could be attenuated further at the damage areas (crack lines and gaps) induced during the earlier loading cycle.

There was no "pop-out" in the unloading *F–d* curve even when a second AE event was detected [Figs. 8(a) and 9(a)]. It was also reported elsewhere that the delamination does not usually lead to a "pop-out" in the *F–d* curves.[32] However, Chang and Zhang reported the "pop-out" observation of the unloading *F–d* curve of the monocrystalline silicon using a Berkovich indenter. They described the "pop-out" as the result of different evolution processes of the phase transformations in the silicon, from Si-II to Si-III/Si-XII and/or to amorphous phases, thus reducing the volume of the residual Si-II zone.[43]

The damage test was then evaluated with a Vickers indenter, where 10 indentations were performed on the Si die. During the loading stage, the "pop-in" was not obvious in the *F–d* curve, where the average onset crack forces measured was ~0.3 N corresponding to the first AE event detected. In the unloading stage, a "pop-out" in the *F–d* curve was observed, as shown in Fig. 12. However there was no AE event detected related to this "pop-out" occurrence, except the one near the end of the unloading stage, which could be related to the chipping of the Si. It is deduced that the AE sensor used in this damage test system is not capable of detecting any phase transformations in Si. It is also interesting to discover that the "pop-out" in the *F–d* curve only happened with a sharp tip indentation but not for a blunt tip, and this observation is still unclear and requires further work to be conducted.

C. Damage test on dielectric stacked structure after top metallization removal

Additional test was evaluated on the specimens without the top metallization layer, with the aim to uncover the damage behavior during unloading. The top Al metallization was etched away to expose the dielectric layers. The loading and unloading rate of 1 N/min was used, and the results are presented in Fig. 13 with the mean onset crack force measured being ~2.1 and ~1.6 N for SiO_2 and Si_3N_4 dielectric specimens, respectively. The results are slightly higher than those for the metal-coated specimens, which could be possibly explained by the different intrinsic or residue stress in the specimen before and after the removal of metallization. Nevertheless, this evaluation attests that the onset crack force is independent of the metal coating.

The radial cracking and chipping were observed on the SiO_2 dielectric surface, and the cone and subsurface cracking was found in the Si substrate, as shown in Fig. 14(a). This is similar to the metal-coated SiO_2 dielectric specimen, where chipping of the SiO_2 layer could be due to the dielectric delamination during the unloading stage. The damage on the Si_3N_4 dielectric specimen is alike to that on the metal-coated Si_3N_4 dielectric specimen, where the radial, ring, and through-thickness cracking was observed in the Si_3N_4 dielectric, and the subsurface cracking was found in the Si substrate [Fig. 14(b)]

https://doi.org/10.1557/jmr.2015.278 Published online by Cambridge University Press

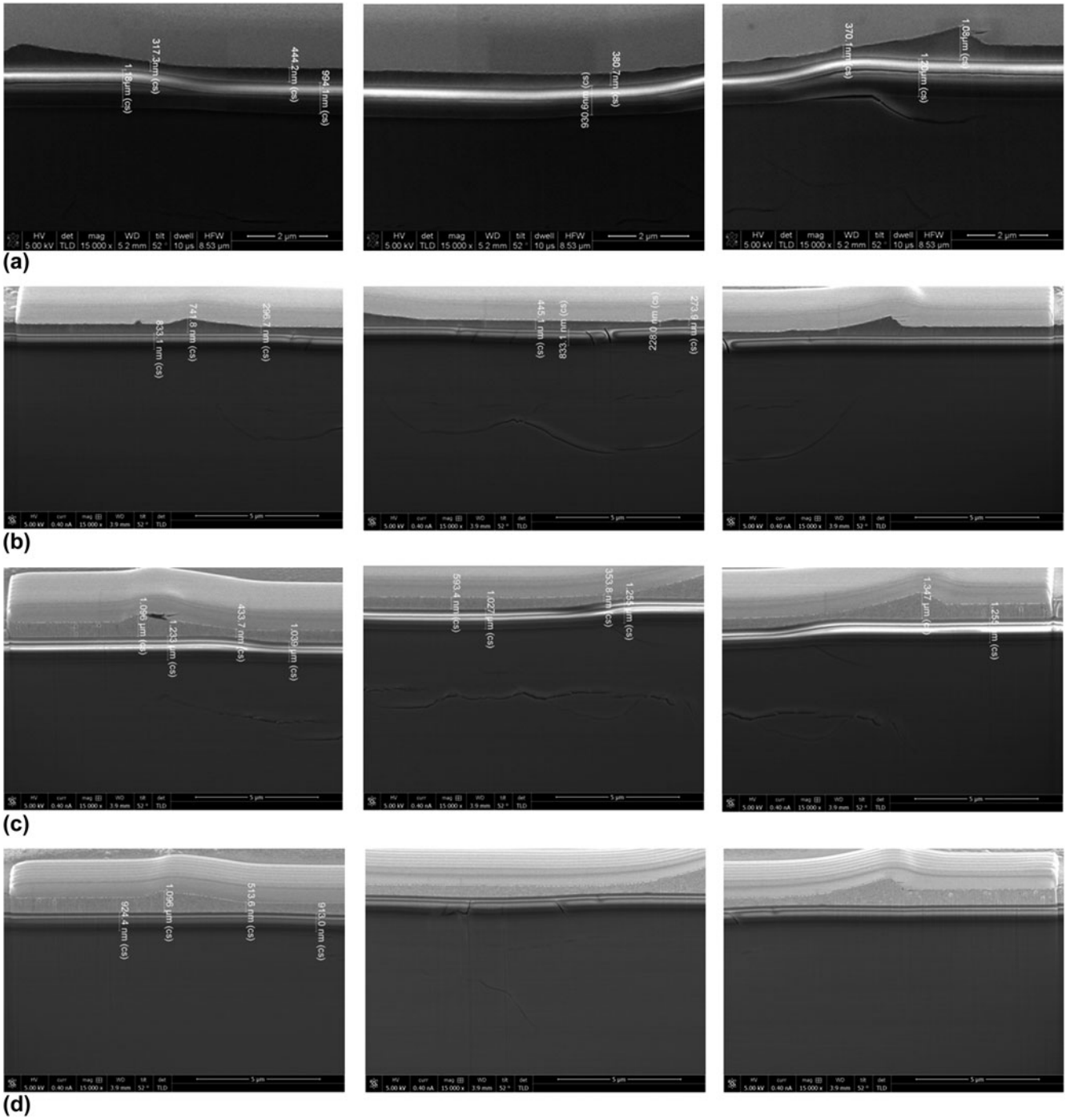


FIG. 11. Cross-sectioning images (FIB/SEM) of the damaged specimens after indentation tests: (a) Al–SiO_2–Si, (b) Al–Si_3N_4–Si, (c) Cu–SiO_2–Si, and (d) Cu–Si_3N_4–Si.

A 2nd AE event was detected during the unloading stage for the SiO_2 dielectric specimen evaluated, which could be due to the delamination and chipping of the SiO_2 layer. However, a few of the indentations on the Si_3N_4 dielectric specimens (<10%) also recorded a 2nd AE event, which is suspected to be the effect of the contact friction between the diamond indenter tip and the damaged and fragmented Si_3N_4 dielectric layer.

D. Indentation damage model of the metal-coated thin-films stacked structure

The damage behavior of the metal-coated thin-films stacked structure is presented in Fig. 15, and for

https://doi.org/10.1557/jmr.2015.278 Published online by Cambridge University Press

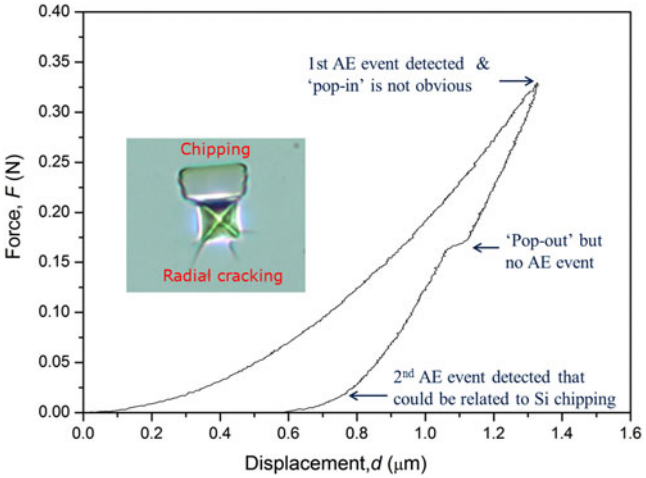


FIG. 12. Indentation F–d curve of the Si die using the Vickers indenter at the 1 N/min loading–unloading cycle, with the insert being the failure image of the indented Si surface.

illustration simplicity the pile-up effect of the top metallization is not drawn here. For the metal-coated SiO_2 dielectric specimen [Fig. 15(a)], the top metallization underwent an elastic–plastic deformation during the loading (stage I), while the dielectric layer and the Si substrate were assumed to be deformed elastically. When the first AE event was detected, the loading stop (stage II) F_{cr} was determined, which corresponded to the peeling and radical cracking on the dielectric surface, and the cone and subsurface cracking in the Si substrate. Immediately, the indenter proceeded to unload, and the stacked structure then underwent an elastic recovery. As the indentation load reduced, a second AE event occurred, which could result in the delamination or interfacial cracking in the dielectric layer and Si substrate (stage III). If the indentation damage test was performed on the exposed SiO_2 dielectric specimen, chipping would occurred. While for the metal-coated Si_3N_4 dielectric specimen

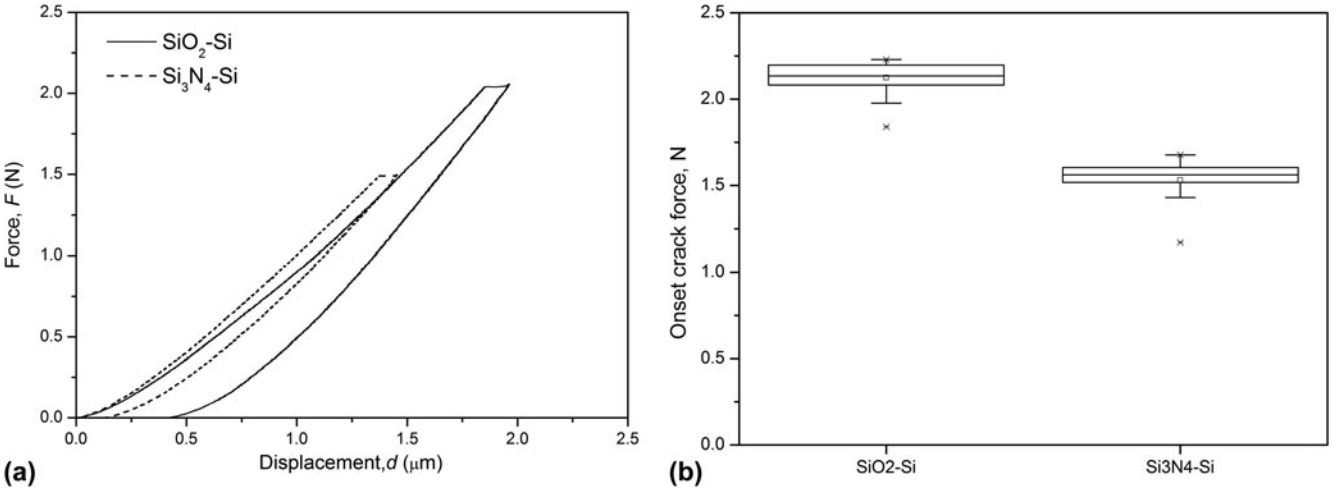


FIG. 13. Mechanical responses of the dielectric layer specimens: (a) indentation F–d response, and (b) onset crack forces.

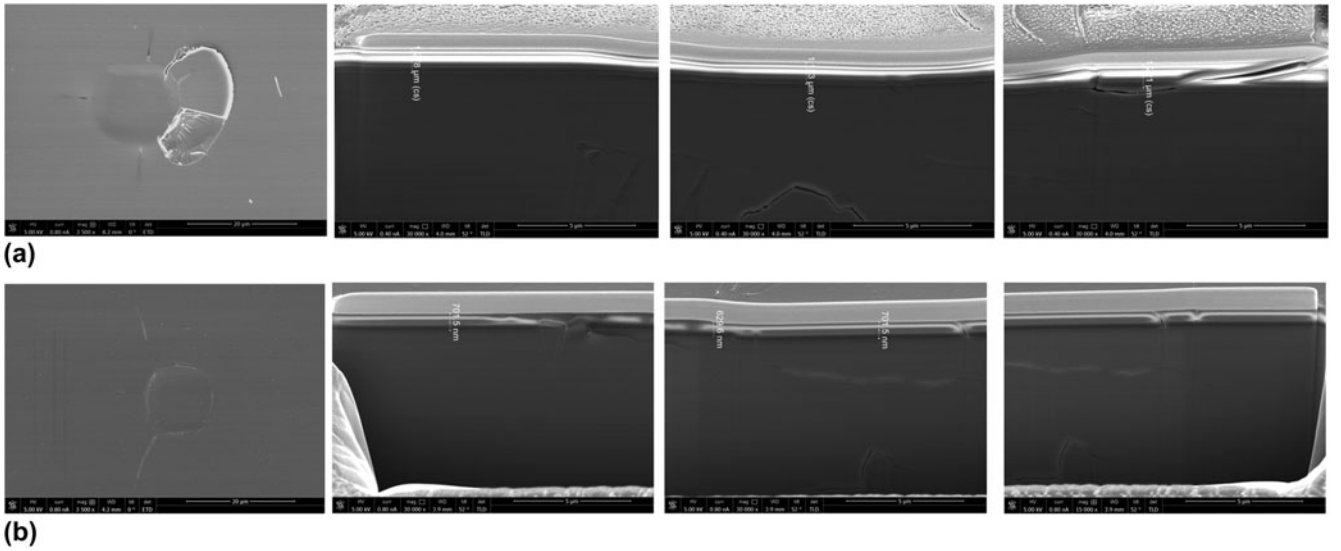


FIG. 14. Cross-sectioning images (FIB/SEM) of the damaged specimens after indentation tests: (a) SiO_2–Si, and (b) Si_3N_4–Si.

https://doi.org/10.1557/jmr.2015.278 Published online by Cambridge University Press

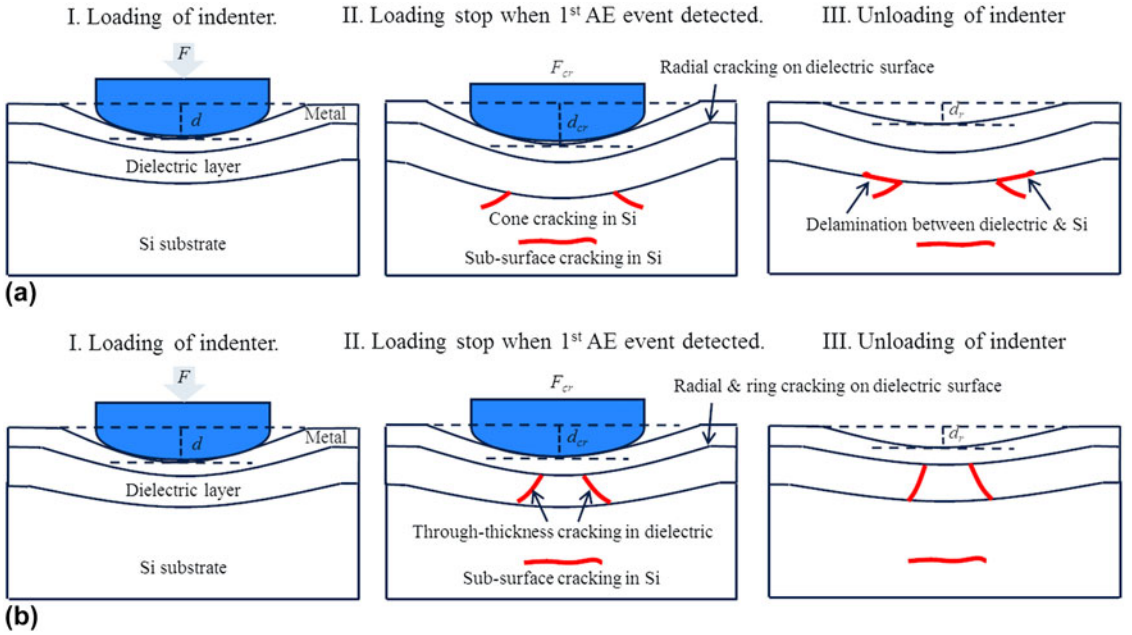


FIG. 15. Indentation damage model for: (a) metal-coated SiO_2 dielectric, and (b) metal-coated Si_3N_4 dielectric on Si substrate.

[Fig. 15(b)], the ring and radial cracking was observed on the dielectric surface, the cone and through-thickness cracking was observed in the dielectric layer, and the subsurface cracking was found in the Si substrate, when the first AE event was detected during the loading stage.

IV. SUMMARY

A damage test methodology invoking the techniques of instrumented indentation testing and AE sensing has been developed to evaluate the metal-coated thin-films stacked structure. The critical load F_{cr} determined corresponds to the 1st AE event occurrence and the "pop-in" in the *F*–*d* curve, which is mainly due to the brittle cracking in the dielectric layer or Si substrate. A lower magnitude of a second AE event is detected, but no "pop-out" is observed in the *F*–*d* curve, which is related to delamination or interfacial cracking between the dielectric layer and the Si substrate. It is also found that "pop-out" during the unloading stage only happens with a sharp indenter tip and is related to the Si phase transformation, but not for a blunt indenter tip. In general, the onset crack force strongly depends on the dielectric layer used, as compared to the metallization layer. Furthermore, a higher onset crack force threshold is usually obtained in the metal-coated SiO_2 dielectric specimen over the metal-coated Si_3N_4 dielectric specimen. Furthermore, delamination only happens in the metal-coated SiO_2 dielectric specimen during the unloading stage.

This study provides an understanding of the indentation damage mechanisms of a soft metal coating over a brittle dielectric material structure. The application be found in the wire bonding process on the bond pad of an integrated circuit (IC) device, where the damage-sensitive pad can be identified and handled with care.[40,41] Furthermore, the methodology can be implemented in terms of design rules or guidelines for the bond pad stack structure, or even as a mechanical screening tool for wafer quality check, which will eventually enable resilient statements for improving product quality and reliability of IC chips.

ACKNOWLEDGMENTS

The authors are grateful to the Failure Analysis colleagues from the Infineon Technologies Asia Pacific and the staff from Micro-machining Lab at Nanyang Technological University for their support in specimen preparation. The authors also acknowledge financial support from Ministry of Education, Singapore (Academic Research Fund TIER 1 - G128/14).

REFERENCES

1. I.N. Sneddon: The relationship between load and penetration in the axisymmetric Boussinesq problem for a punch of arbitrary profile. *Int. J. Eng. Sci.* **3**, 47–57 (1965).
2. B.R. Lawn and R. Wilshaw: Review indentation fracture: Principles and applications. *J. Mater. Sci.* **10**, 1049–1081 (1975).
3. B.R. Lawn and D.B. Marshall: Indentation fracture and strength degradation in ceramics. *Fract. Mech. Ceram.* **3**, 205–229 (1975).
4. B.R. Lawn and D.B. Marshall: Hardness, toughness, and brittleness: An indentation analysis. *J. Am. Ceram. Soc.* **62**(7–8), 347–350 (1979).
5. B.R. Lawn, A.G. Evans, and D.B. Marshall: Elastic/plastic indentation damage in ceramics: The median/radial crack system. *J. Am. Ceram. Soc.* **63**(9–10), 574–581 (1980).

https://doi.org/10.1557/jmr.2015.278 Published online by Cambridge University Press

6. G.R. Anstis, P. Chantikul, B.R. Lawn, and D.B. Marshall: A critical evaluation of indentation techniques for measuring fracture toughness. I. Direct crack measurements. *J. Am. Ceram. Soc.* **64**(9), 533–538 (1981).
7. G.R. Anstis, P. Chantikul, B.R. Lawn, and D.B. Marshall: A critical evaluation of indentation techniques for measuring fracture toughness. II. Strength method. *J. Am. Ceram. Soc.* **64**(9), 539–543 (1981).
8. M.F. Doerner and W.D. Nix: A method for interpreting the data from depth-sensing indentation instruments. *Journal of Material Research* **1**, 601–609 (1986).
9. W.C. Oliver and G.M. Pharr: An improved technique for determining hardness and elastic modulus using load and displacement sensing indentation measurements. *J. Mater. Res.* **7**, 1564–1583 (1992).
10. M. Sakai: Energy principle of the indentation-induced inelastic surface deformation and hardness of brittle materials. *Acta Mater.* **41**(6), 1751–1758 (1993).
11. D.S. Harding, W.C. Oliver, and G.M. Pharr: Cracking during nanoindentation and its use in the measurement of fracture toughness. *Mater. Res. Soc. Proc.* **356**, 663–668 (1995).
12. C.M. Cheng and Y.T. Cheng: On the initial unloading slope in indentation of elastic-plastic solids by an indenter with an axisymmetric smooth profile. *Appl. Phys. Lett.* **71**, 2623 (1997).
13. G.M. Pharr: Measurement of mechanical properties by ultra-low load indentation. *Mater. Sci. Eng., A* **253**, 151–159 (1998).
14. Y.T. Cheng and C.M. Cheng: Relationships between hardness, elastic modulus, and the work of indentation. *Appl. Phys. Lett.* **73** (5), 614–616 (1998).
15. X.Z. Hu and B.R. Lawn: A simple indentation stress–strain relation for contacts with spheres on bilayer structures. *Thin Solid Film* **322**, 225–232 (1998).
16. J. Alcala, F. Gaudette, S. Suresh, and S. Sampath: Instrumented spherical micro-indentation of plasma-sprayed coatings. *Mater. Sci. Eng., A* **316**, 1–10 (2001).
17. A.A. Volinsky, B.J. Vella, and W.W. Gerberich: Fracture toughness, adhesion and mechanical properties of low-*K* dielectric thin films measured by nanoindentation. *Thin Solid Films* **429**, 201–210 (2003).
18. M.R. VanLandingham: Review of instrumented indentation. *J. Res. Natl. Inst. Stand. Technol.* **108**, 249–265 (2003).
19. W.C. Oliver and G.M. Pharr: Measurement of hardness and elastic modulus by instrumented indentation: Advances in understanding and refinements to methodology. *J. Mater. Res.* **19**(1), 1–20 (2004).
20. K.J. Van Vliet, L. Prchlik, and J.F. Smith: Direct measurement of indentation frame compliance. *J. Mater. Res.* **19**, 325–333 (2004).
21. A.R. Franco, Jr., G. Pintaúdeb, A. Sinatoraa, C.E. Pinedoc, and A.P. Tschiptschina: The use of a vickers indenter in depth sensing indentation for measuring elastic modulus and vickers hardness. *Mater. Res.* **7**(3), 483–491 (2004).
22. Z.H. Xia, W.A. Curtin, and B.W. Sheldon: A new method to evaluate the fracture toughness of thin films. *Acta Mater.* **52**, 3507–3517 (2004).
23. Y-G. Jung, B.R. Lawn, M. Martyniuk, H. Huang, and X.Z. Hu: Evaluation of elastic modulus and hardness of thin films by nanoindentation. *J. Mate. Res.* **19**(10), 3076–3080 (2004).
24. S. Chen, L. Liu, and T. Wang: Investigation of the mechanical properties of thin films by nanoindentation, considering the effects of thickness and different coating–substrate combinations. *Surf. Coat. Technol.* **191**, 25–32 (2005).
25. L.M. Farrissey and P.E. McHugh: Determination of elastic and plastic material properties using indentation: Development of method and application to a thin surface coating. *Mater. Sci. Eng., A* **399**, 254–266 (2005).
26. F. Helvaci and J. Cho: A nanoindentation study of thermally-grown-oxide films on silicon. *Mater. Res. Soc. Symp. Proc.* **841**, 375–380 (2005).
27. I. Etsion, Y. Kligerman, and Y. Kadin: Unloading of an elastic–plastic loaded spherical contact. *Int. J. Solids Struct.* **42**, 3716–3729 (2005).
28. Y.Y. Lim and M.M. Chaudhri: Indentation of elastic solids with a rigid Vickers pyramidal indenter. *Mech. Mater.* **38**, 1213–1228 (2006).
29. J.S. Lee, J. Jang, B.W. Lee, Y. Choi, S.G. Lee, and D. Kwon: An instrumented indentation technique for estimating fracture toughness of ductile materials: A critical indentation energy model based on continuum damage mechanics. *Acta Mater.* **54**, 1101–1109 (2006).
30. F. Sergejev and M. Antonov: Comparative study on indentation fracture toughness measurements of cemented carbides. *Proc. Est. Acad. Sci. Eng.* **12**(4), 388–398 (2006).
31. J. Chen and S.J. Bull: Assessment of the toughness of thin coatings using nanoindentation under displacement control. *Thin Solid Films* **494**(1–2), 1–7 (2006).
32. J. Chen and S.J. Bull: Modelling the limits of coating toughness in brittle coated systems. *Thin Solid Films* **517**(9), 2945–2952 (2009).
33. J.J. Kruzica, D.K. Kimb, K.J. Koesterc, and R.O. Ritchiec: Indentation techniques for evaluating the fracture toughness of biomaterials and hard tissues. *J. Mech. Behav. Biomed. Mater.* **2**, 384–395 (2009).
34. J. Chen: Indentation-based methods to assess fracture toughness for thin coatings. *J. Phys. D: Appl. Phys.* **45**(20), 1–14 (2012).
35. S. Zhang and X.M. Zhang: Toughness evaluation of hard coatings and thin films. *Thin Solid Films* **520**, 2375–2389 (2012).
36. S. Kucharski and Z. Mroz: Identification of yield stress and plastic hardening parameters from a spherical indentation test. *Int. J. Mech. Sci.* **49**, 1238–1250 (2007).
37. W.Y. Yan, Q.P. Sun, and D.P. Hodgson: Determination of plastic yield stress from spherical indentation slope curve. *Mater. Lett.* **62**, 2260–2262 (2008).
38. S-K. Kang, J-Y. Kim, C-P. Park, H-U. Kim, and D. Kwon: Conventional Vickers and true instrumented indentation hardness determined by instrumented indentation tests. *J. Mater. Res.* **25**(2), 337–343 (2010).
39. A.C. Fischer-Cripps: *Nanoindentation*. 3rd ed. (Springe, New York, 2011).
40. A. Yeo, E. Yong, S.T. Dan, and G.M. Ruether: A novel damage test evaluation of IC bond pad stack strength. In *Proceedings of 15th Electronics Packaging Technology Conference*; IEEE, Singapore, 2013; pp. 40–43.
41. A. Yeo, E. Yong, and K. Zhou: Compliance compensation analysis of micromechanical tester integrated with acoustic emission sensors. *IEEE Trans. Device Mater. Reliab.* **14**(3), 898–903 (2014).
42. M.J. Madou: *Fundamentals of Microfabrication* (CRC Press, Boca Raton, FL, 1997).
43. L. Change and L.C. Zhang: Deformation mechanisms at pop-out in monocrystalline silicon under nanoindentation. *Acta Mater.* **57**, 2148–2153 (2009).

https://doi.org/10.1557/jmr.2015.278 Published online by Cambridge University Press